

# Interference analysis and modeling of Positioning Reference Signals in 5G NTN

Alejandro Gonzalez-Garrido\*, *Student, IEEE*, , Jorge Querol\*, *Member, IEEE*, , Henk Wymeersch†, *Fellow, IEEE*, , Symeon Chatzinotas\*, *Fellow, IEEE*, 

\*Interdisciplinary Centre for Security, Reliability and Trust. SnT. University of Luxembourg

†Department of Electrical Engineering, Chalmers University of Technology

Corresponding author: Alejandro Gonzalez-Garrido, e-mail: alejandro.gonzalez@uni.lu

This work has been submitted to the IEEE for possible publication. Copyright may be transferred without notice, after which this version may no longer be accessible

## ABSTRACT

The integration of Positioning, Navigation, and Timing (PNT) services within the 5G non-terrestrial network (NTN) infrastructure is required to remove the requirement of a GNSS receiver in the user terminal. Using the positioning reference signal (PRS) in an NTN scenario presents significant challenges such as interference analysis from the transmission of several PRS. This study provides a stochastic model for the interference generated by PRS transmissions in a 5G NTN scenario. This model has been extracted empirically from a Monte Carlo simulator designed ad hoc for this purpose, showing the distribution that better fits the interference is a Generalized Extreme Value (GEV) distribution. The parameters of this distribution are also modeled in terms of the PRS configuration. Therefore, a designer can use this model to evaluate the probability of having certain levels of interference.

**INDEX TERMS** 5G, NTN, PNT, PRS, interference, SINR, GEV distribution.

## I. Introduction

ONE key reason for extending fifth generation (5G) services to non-terrestrial network (NTN) scenarios is the pursuit of global coverage for data services. From Release-17, NTN user equipments (UEs) were mandated to incorporate a global navigation satellite system (GNSS) receiver to access NTN services [1]. However, this requirement poses challenges for satellite network operator (SNO), as it limits their ability to offer their services in GNSS denial areas. Furthermore, the power consumption of GNSS receivers in Internet of things (IoT) devices could compromise their commercial viability. Consequently, developing a GNSS-free UE for NTN operation is critical, motivating this study to explore offering positioning, navigation, and timing (PNT) services alongside data services through a unified NTN infrastructure. 3rd Generation Partnership Project (3GPP) in its release-16 of 5G has standardized positioning features to

offer PNT services [2]. These features are distinguished by the deployment of various positioning techniques. Among the various positioning techniques in 5G, the use of a specific downlink signal, positioning reference signal (PRS), is notable because it offers a wider bandwidth and higher carrier frequencies compared to previous generations, reaching up to 100 MHz in frequency region 1 (FR1) band and up to 400 MHz in frequency region 2 (FR2) band [3], [4]. However, the current definition of 5G PNT services necessitates a network connection for the subscriber; in other words, 5G PNT services are on-demand by the UE, the core network, or a third party connected to the core network, in contrast to GNSS that is a broadcast service. This architecture, inherited from Long Term Evolution (LTE), was initially designed for emergency call requirements as a terrestrial positioning system. In this framework, the network informs the UE about the PRS configuration; subsequently,

the UE acquires and relays the measurements back to the core network, which then performs position estimation. This approach poses scalability challenges in terms of the number of simultaneous users. In addition, the 5G networks, from release-17 onward, include NTN elements such as unmanned aerial vehicle (UAV), high-altitude platform systems (HAPS), and satellites. These components, increasingly emphasized by industry stakeholders, facilitate global communication capabilities [5]. Furthermore, in a NTN satellite scenario each UE require position information prior to its initial access. Therefore, current standardized positioning techniques are impractical due to the prerequisite of network connection for UE. Going beyond 5G, the 6G network is expected to establish a unified network entity, characterized by multiple connectivity layers designed to meet various device requirements in various scenarios [6]. Therefore, the convergence of network's PNT services with NTN offers numerous advantages. These include the development of an autonomous integrated communication and navigation system under a unified network infrastructure, enhanced accuracy in PNT solutions surpassing previous generations, global coverage that allows synchronized navigation and communication, increased resilience to positioning estimation, and the emergence of innovative services [7]. In addition, recent studies highlight the technological potential to achieve a truly integrated communication, location, and sensing system [8]. Furthermore, industry is also pushing forward, with the development of the Xona service, the LEO-PNT mission from ESA, and the Geosat constellation from ESA and China. However, these commercial development do not include a communication service.

### **A. State of the Art**

Although the integration of communication and navigation systems within a unified network, as highlighted in the previous paragraph, holds the promise of revolutionizing PNT solutions, it also introduces new challenges in signal interference management. The literature on interference in orthogonal frequency-division multiplexing (OFDM) systems, as illustrated [9]–[11], focuses mainly on terrestrial communication scenarios, focusing on inter-symbol interference (ISI) issues in multipath environments. This existing research is pivotal for understanding interference dynamics; however, it mainly explores scenarios involving single transmitters. Furthermore, studies [12], [13] delve into inter-numerology interference (INI) modeling and improvement strategies, primarily in single-transmitter scenarios with inter-carrier interference (ICI), ISI, and INI as the main aggressors. The complexity increases multifold when considering integrated systems, where multiple transmitters and receivers interact within a shared spectral environment. Similar approaches are already available in the literature for terrestrial networks, such as [14] where they proposed a fraction frequency reuse (FFR) scheme, or the concept of Network-MIMO, developed in [15] for indoor scenarios.

However, none of them are intended for navigation systems. Therefore, this requires the development of advanced interference management techniques that can cater to the unique requirements of an integrated communication and navigation system, ensuring the reliability and accuracy essential for such a converged network infrastructure [16]. This gap in existing research underscores the need for comprehensive studies that extend beyond traditional interference models to address the intricacies of integrated systems in future networks. In a satellite scenario, the delays between the signals from different satellites (ms order) significantly exceed the length of the cyclic prefix (CP) of the waveform ( $\mu$ s order) [17]. This leads to ISI and ICI at the receiver located in areas of overlapping inter-satellite beams. Assuming that all satellites are synchronized and that all satellites send positioning pilots synchronously in the same bandwidth part (BWP), two strategies are considered in the literature to address interference. The satellites apply a temporal guard band (called muting [18]) long enough for the signal to reach each beam edge, or the satellites exploit the low probability of signal collision due to the large differential delay between satellites [19]. Despite significant advancements in interference analysis for 5G NTN scenarios, a critical area remains underexplored: the aggregated interference effects caused by positioning signal transmissions, such as the PRS, within an NTN context. Current research does not thoroughly investigate the interference generated by differential propagation delays between satellites, which are considerably longer than the PRS slot duration [17]. It is essential for system designs to ensure that the interference levels between PRS and data transmissions are minimized, allowing the receiver to accurately decode the data symbols and extract the observables of positioning. This area of study is crucial for the development and optimization of PNT services. By meticulously characterizing interference phenomena and understanding their impact on received signals, we can develop robust positioning algorithms and techniques that effectively mitigate interference effects. This will greatly improve the accuracy and reliability of positioning services, addressing the growing need for precision in contemporary applications.

### **B. Paper Contributions**

In this paper, we evaluate the signal to interference plus noise ratio (SINR) degradation due to multiplexing the broadcasting of PRS among different satellite next generation base station (gNB)s in a BWP. We assume the terrestrial multiplexing scheme for the PRS signals [20] and translate it into a NTN scenario. Our proposal adopts an approach similar to that used by GNSS, utilizing a dedicated BWP for broadcasting the PRS, termed bandwidth part for positioning (BWPP). Within the BWPP the network operator broadcast the PRS across all satellites. This requires a comprehensive analysis of the generated interference, ensuring that it remains sufficiently low for the receiver to decode the data symbols. Our study proposes an evaluation of interference

in a system broadcasting positioning signals in a dedicated BWP, therefore these signals are accessible to all users, similar to GNSS. This approach enables UEs to initiate initial access to NTN without requiring a GNSS receiver. The primary objective of this research is to model the interference power received by a user terminal on the ground. The study focuses on the statistical characteristics of interference, critical for UE positioning estimation. The contributions of this study include the following.

- 1) Conducting a theoretical analysis of the received signal and the interference generated by the simultaneous reception of 4 PRS at the receiver side. This interference is calculated at the output of the matched filter at the receiver.
- 2) Develop a Monte Carlo simulator to evaluate the interference generated by the PRS. The PRS can be configured for a different number of symbols, comb-size and transmitted power. It outputs the delay/Doppler map (DDM) as a matched filter at the receiver for all received signals.
- 3) Extract a novel stochastic model of the interference generated by the PRS. This model is based on the configuration of the PRS such as the transmitted power, the number of symbols, and the comb-size used at the transmitter side. The model fitting is performed empirically with the results from the Monte Carlo simulator designed previously.

The structure of this paper is as follows. Section II details the scenario and the channel model for low Earth orbit (LEO). Section III presents the signal models used in NTN, the matched filter at the receiver, and the interference model. Section IV shows the Monte Carlo simulator developed and the stochastic model of interference extracted from the simulation results. Finally, Section V discusses the conclusions drawn from this study and suggests directions for future research.

## II. Scenario for 5G Satellite Positioning

This section outlines the framework and scenario definition for a PNT service provision via 5G NTN. Involves a detailed examination of assumptions, simplifications, and the reasoning behind them. The proposed model requires that the signal from at least four distinct NTN gNBs similar to GNSS reaches the user terminal. In our study, we adopt an Earth-moving beam configuration, where the satellite beam moves along the satellite, as defined in 3GPP TR 38.821. without loss of generality, as the interference will be analyzed for single snapshot estimations. For multibeam satellites, the satellite implements precompensation at a reference ground point for each beam, effectively reducing the maximum delay/Doppler range experienced by the signal. Consequently, a single beam satellite represents a worst-case scenario from this perspective, which we focus on in our analysis. Nowadays, beams overlapping can be fulfilled by

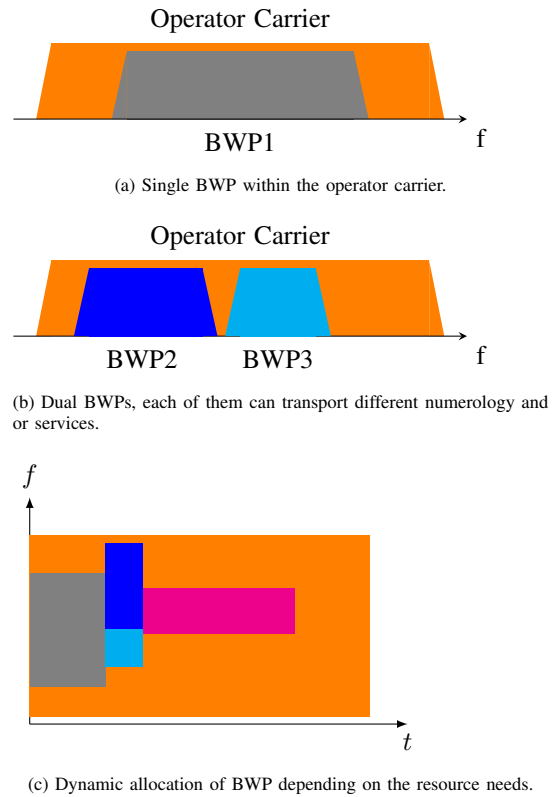


Figure 1: Split of operator spectrum in different BWP in frequency and time.

massive constellations such as Starlink (our case assumes a single shell where all satellites are at the same altitude). There are some examples in the literature such as [21] on how to achieve this beam overlapping for a data service.

### A. Frequency reuse in a common 5G Resource Grid

In a positioning system, the UE has to receive several signals to obtain the observables. In the case of a 3D position using time of arrival (ToA) the UE must receive the PRS from at least four satellites to estimate its state as: position and clock bias,  $[x, y, z, \delta(t)]$ . A multiplexing scheme must be devised to address the high delays and Doppler shift characteristic of the NTN channel, ensuring that the user can receive all four signals with minimal aggregate interference. In this regard, a 5G network operator can dynamically allocate its physical resources (time and frequency) based on the requirements of the user case. This dynamic allocation is referred to as BWP, wherein the signals for different user profiles are partitioned in frequency or time, depending on the resources requested or available, as illustrated in Figure 1.

In this study, we implement the PRS multiplexing design used for terrestrial applications [20], depicted in Figure 2. This design facilitates the transmission of multiple PRS within a single OFDM slot, whereby the empty resource element (RE) left by one transmitter, due to the steps of the

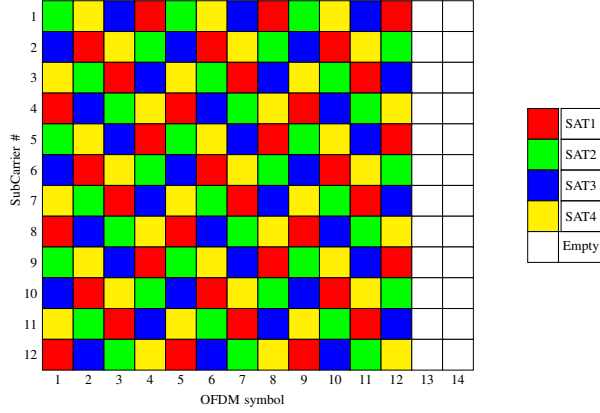


Figure 2: 5G PRS Transmitted Resource Grid example to multiplex 4 different satellites (each color is the PRS transmission from a different satellite). Size 1 Resource Block  $\times$  1 Slot and a Comb Size (frequency periodicity of the PRS per transmitter) of 4.

subcarrier (“CombSize” parameter), is used by another gNB for their PRS allocation.

Unlike the terrestrial channel, the NTN channel experiences larger differential delays and Doppler shifts. Our analysis is focused on the interference generated by different transmissions in this scenario, where each satellite’s signal travels through a wireless channel that can be assumed to be independent and uncorrelated for each satellite. A challenge in this scenario is to minimize interference between transmissions from different satellites.

### B. Satellite Scenario

The initial step in evaluating a satellite system involves determining the service requirements, which, in turn, establishes a minimum SINR at the perimeter of the service beam. Achieving this required SINR primarily depends on mitigating the loss of the link, where the key factor is the distance between the satellite and the user at the edge of the beam marked as  $\rho_{MAX}$  in Figure 3. This distance is essential to close the link budget.

Figure 3 shows the field of view (FoV) of a satellite. Here, the furthest boundary represents the complete view of Earth from a satellite when a user is positioned at an elevation angle of  $0^\circ$ . It also delimits the maximum area of coverage by a radius  $R_{MAX}$ . At the center of this illustration lies the subsatellite point (SSP), which is the perpendicular projection of the satellite position on the Earth’s surface. The dashed circle in Figure 3 delimits the coverage area when users limit its operation to a certain elevation angle mask  $\theta_{MASK}$ , due to link budget constraints. The value of  $\theta_{MASK}$  is crucial as it significantly impacts the maximum signal propagation time between the satellite and the ground station, as well as the maximal losses incurred due to free space path loss (FSPL).

Figure 4 shows as a perpendicular cross section of the plane illustrated in Figure 3, aiding in understanding the

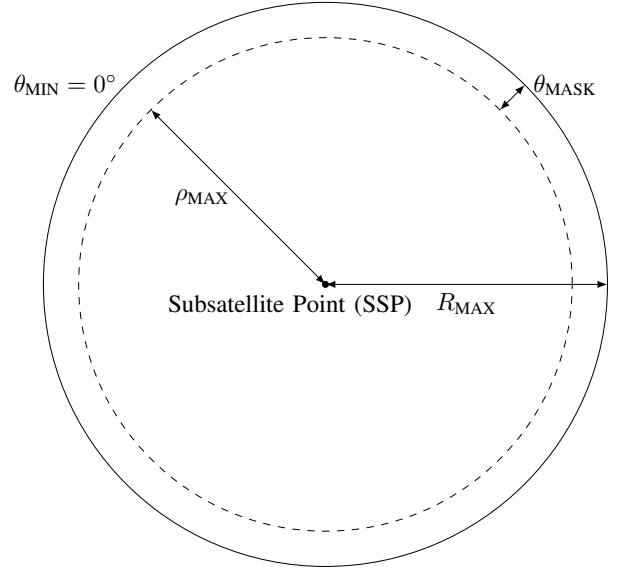


Figure 3: Satellite maximum Field of View (FoV) (circle where the elevation angle mask is  $0^\circ$ ). And satellite useful FoV (dashed circle) depends on the selected elevation angle mask  $\theta_{MASK}$  and defines the maximum distance satellite-user  $\rho_{MAX}$ .

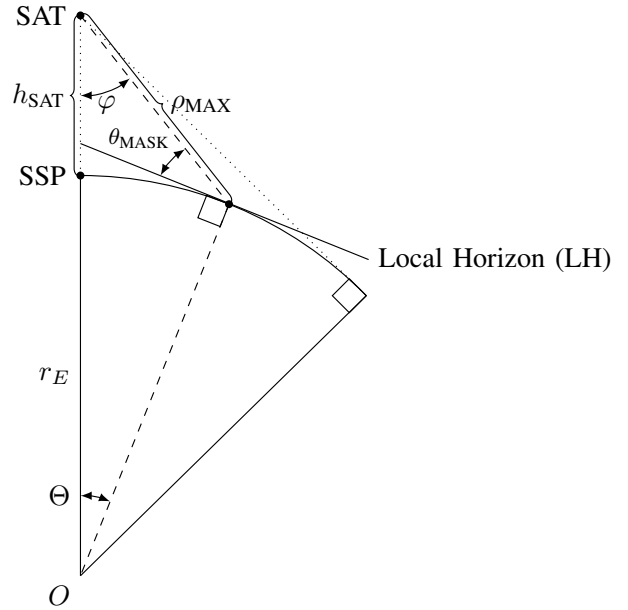


Figure 4: Distances and angles within a satellite beam depends on the user local horizon (LH), and the altitude of the satellite  $h_{SAT}$ .

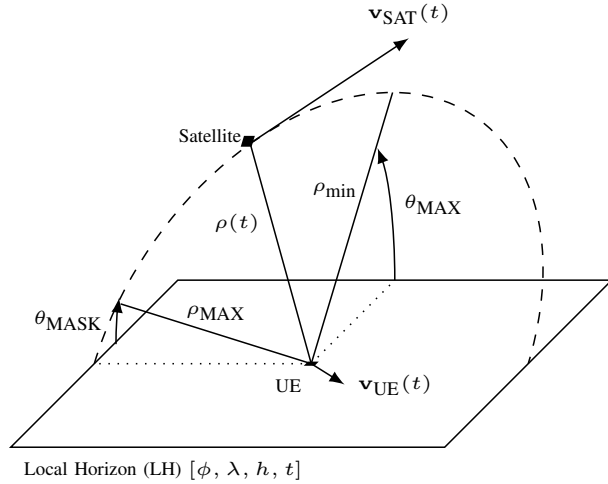


Figure 5: Parameters involved in a single satellite pass.

trigonometric calculations leading to (1). This figure demonstrates the direct relationship between  $\theta_{\text{MASK}}$  and  $\rho_{\text{MAX}}$ , in relation to the altitude of a satellite  $h_{\text{SAT}}$  plus the radius of the Earth  $r_E$ .

$$\rho_{\text{MAX}} = (r_E + h_{\text{SAT}}) \frac{\sin\left(\frac{\pi}{2} + \Psi\right)}{\sin\left(\frac{\pi}{2} + \theta_{\text{MASK}}\right)} \quad (1)$$

With the value of  $\Psi$  defined as:

$$\Psi = -\theta_{\text{MASK}} - \arcsin\left(\frac{r_E \sin\left(\frac{\pi}{2} + \theta_{\text{MASK}}\right)}{r_e + h_{\text{SAT}}}\right)$$

Besides, the Local Horizon (LH) is the perpendicular plane to the Earth surface, at the user location, used to define the parameters of a satellite pass over this user.

Figure 5 presents a three-dimensional representation of a single satellite pass, which is an expansion of the concept of LH from Figure 4. This depiction emphasizes that LH depends on the geographical coordinates of the user, defined by latitude  $\phi$ , longitude  $\lambda$ , altitude above mean sea level  $h$ , and time of observation  $t$ . This implies that a moving user's LH will change over time. However, for our analysis, as the user speed  $\mathbf{v}_{\text{UE}}(t) \ll \mathbf{v}_{\text{SAT}}(t)$  is much smaller than the satellite speed, we could assume the user is static. Moreover, Figure 5 highlights various parameters that play a critical role in understanding satellite dynamics from the perspective of a ground user, which are integral to the channel model. Among these parameters,  $\theta_{\text{MAX}}$  stands out as particularly significant. It represents the maximum elevation angle that the satellite will attain during a specific pass over the user. This parameter is vital because it influences several other factors, such as the duration of the satellite pass and the minimum distance between the satellite and the user, represented by  $\rho_{\text{min}}$ . The range of  $\theta_{\text{MAX}}$  is defined as being between  $[\theta_{\text{MASK}}, \pi/2]$ . It should be noted that each satellite pass will have a unique value of  $\theta_{\text{MAX}}$ , which is determined by orbital dynamics and the specific location of the user.

### C. Wireless Channel Model

We use a delay/Doppler spread representation of the wireless channel [22], i.e.,

$$\gamma_i(v, \tau) = \sqrt{L_i} h_i \delta(v - v_i) \delta(\tau - \tau_i). \quad (2)$$

The channel representation in (2) depends on 4 parameters: the free space path losses  $L_i = (c/(4\pi f_c \rho_i))^2$ , a random phase rotation  $h_i$ , a delay  $\tau_i = \rho_i/c$  and a Doppler shift defined as  $v_i \triangleq -\frac{f_c}{c} \frac{d}{dt} \rho_i$ . Where  $\rho_i = \|\mathbf{r}_{\text{SAT}_i} - \mathbf{r}_{\text{UE}}\|$  is the distance between UE and  $i$ -th satellite,  $\frac{d}{dt} \rho_i = \hat{\mathbf{u}}_{\text{SAT}_i}^T \mathbf{v}_{\text{SAT}_i, \text{UE}}$  is the relative speed between the UE and  $i$ -th satellite calculated as the projection of  $\mathbf{v}_{\text{SAT}_i, \text{UE}}$  in  $\hat{\mathbf{u}}_{\text{SAT}_i}$ . Then,  $\hat{\mathbf{u}}_{\text{SAT}_i} = \frac{\mathbf{r}_{\text{SAT}_i} - \mathbf{r}_{\text{UE}}}{\|\mathbf{r}_{\text{SAT}_i} - \mathbf{r}_{\text{UE}}\|}$  is a unitary vector that points from the user to the  $i$ -th satellite, and  $\mathbf{v}_{\text{SAT}_i, \text{UE}} = (\mathbf{v}_{\text{SAT}_i} - \mathbf{v}_{\text{UE}})$  is the vector of velocity difference. The channel FSPL is modelled by  $L_i$  assuming a unit gain on the TX and RX antennas. It depends on the carrier frequency  $f_c$ , and  $\rho_i$ . A more realistic NTN channel has other losses, such as tropospheric effects (gas absorption, rain/cloud attenuation), antenna beam/polarisation misalignment, etc. These effects are assumed negligible as these attenuations compared to FSPL are much lower for transmissions in L/S frequency bands. The signal delay  $\tau_i$  is also considered constant, as the change during a slot is negligible. A more accurate model would include an excess of ionospheric and tropospheric delay due to signal refraction. These effects have been extensively studied for GNSS receivers and are modelled by the Klobuchar model [23] or the NeQuick model [24], [25]. However, the inclusion of these models could obscure the analysis of this work that focuses on the effects on the performance of the satellite dynamics. The model of  $v$  shows that the measured Doppler is proportional to the relative speed of the satellite-user link in an ideal scenario, where its value is only affected by the dynamics of the satellite and the user. The channel model in (2) will serve as a baseline for the generation of a dataset published in [26]. This dataset has several user positions, and for each location several satellite passes are computed with 1 second resolution. For each pass, the satellite position and velocity are stored. Furthermore, we assume that the channel is wide-sense stationary (WSS) for the duration of the slot (10 ms), thus, the values of  $L_i$ ,  $\tau_i$ , and  $v_i$  can be considered constant for the duration of the slot. This is a realistic assumption that does not compromise the results, as similar NTN models use it [27].

### III. Transmitted and received signal model

In this section, we present the transmitted signal model and the theoretical framework for analyzing interference between satellites transmitting the PRS. Our focus is on analyzing the impact of the NTN channel on transmissions from  $S$  satellites, assuming line of sight (LOS) and no multipath effects.

#### A. Downlink Signal Model

The 5G downlink signal model begins with the generation of the PRS sequence for each  $i$ -th satellite. This sequence is

then mapped onto the resource grid (RG) in accordance with 3GPP TS 38.211 Section 7.4.1.7.3 [28] as  $\mathbf{A}_i \in \mathbb{C}^{M \times N_{\text{SCS}}}$  where  $M$  are the OFDM symbols and  $N_{\text{SCS}}$  the total number of subcarriers of the Resource Grid. The cyclic prefix orthogonal frequency-division modulation (CP-OFDM) modulation is applied by incorporating zero padding prior to the inverse fast Fourier transform (IFFT) operation as per 3GPP TS 38.211 Section 5.3.1 [28]. Following this, the CP is appended by the transmitter. The transmitted signal from satellite  $i$  is thus expressed in its complex baseband form, as described by

$$x_i(t) = \sqrt{P_{\text{TX}}} \sum_{m=0}^{M-1} \sum_{k=0}^{N_{\text{SCS}}-1} A_i[m, k] e^{j2\pi k \Delta f t} \text{rect}\left(\frac{t - mT_s}{T_s}\right), \quad (3)$$

where  $T_s = T + T_{\text{CP}}$  indicates the symbol duration as the OFDM symbol time  $T$  plus the duration of the CP  $T_{\text{CP}}$ ,  $\Delta f = 1/T$  is the subcarrier spacing, and  $\text{rect}(t/T_s)$  is the rectangular function. We assume the use of the rect pulse as it reduces the computational complexity and maintains the orthogonality between subcarriers, therefore the interference is due to the channel dynamics only.

The transmitted signal  $x_i(t)$  has an average power level of  $P_{\text{TX}}$ . This power level is fixed at the satellite high power amplifier (HPA) to guarantee minimum performance for beam edge users. This approach assumes, akin to GNSS, a uniform equivalent isotropic radiated power (EIRP) across the satellite beam.

### B. Received Signal Model

The channel model outlined in (2) describes a channel between the  $i$ -th satellite gNB and the UE. In a positioning system, the user typically receives all downlink signals within the same BWPP spectrum. Thus, the received signal model is an aggregation of different NTN signals, each affected by a distinct channel  $\gamma_i$ . The received signal is modeled by

$$y(t) = \sqrt{L_i} \sum_{i=0}^{S-1} e^{j2\pi v_i t + \theta} x_i(t - \rho_i/c) + w(t), \quad (4)$$

as the aggregation of the signal received by the  $S$  satellites in LOS. The model (4) is essential for subsequent analyses, including SINR evaluations and performance assessments of the delay estimator.

### C. Matched filter

In the receiver architecture, the matched filter operation is based on the cross ambiguity function (CAF). This process involves correlating the received signal  $y(t)$  with the different pilot signals shifted in frequency certain known value, analogous to the procedure employed by a GNSS receiver in its acquisition phase. The definition

$$\chi_{xy}(v, \tau) = \int_{-\infty}^{+\infty} x(t) y^*(t - \tau) e^{j2\pi v t} dt. \quad (5)$$

illustrates the principle of detector operation, where the received signal is compared against the different local copies of the PRS, one per satellite; therefore, the receiver will perform at least 4 different CAF computations.

Substituting the received signal  $y(t)$  into the CAF, and following a similar analysis done in [29], the matched filter output for the  $i$ -th PRS is given by

$$\begin{aligned} \chi_{yx}^{(i)}(v, \tau) &= \sqrt{L_i} e^{j2\pi(v-v_i)\tau_i} \chi_{xx}^{(i)}(v - v_i, \tau - \tau_i) \\ &+ \sum_{\substack{s \neq i \\ s \geq 0}}^{\text{Sat}-1} \sqrt{L_s} e^{j2\pi(v-v_s)\tau_s} \chi_{xx}^{(i)}(v - v_s, \tau - \tau_s) \\ &+ \chi_{wx}^{(i)}(v, \tau). \end{aligned} \quad (6)$$

### D. Post-matched filter Signal-to-Noise Plus Interference Ratio Analysis

This subsection concludes the modeling discussion by presenting SINR as a critical key performance indicator (KPI) to analyze receiver performance. Assessing SINR is paramount for the effective detection of the peak in the receiver's detector. We know that the maximum value of the ambiguity function (AF) is at the origin  $\tau = 0, v = 0$ , applying a variable change in (6) as  $\tau' = \tau - \tau_i$  and  $v' = v - v_i$  we displace the origin to the peak, then we evaluate the CAF in relation to the difference in delay and Doppler of interference signals. For this we apply the following change of variable in (6)  $\Delta\tau_s = \tau_i - \tau_s$  and  $\Delta v_s = v_i - v_s$ , yielding

$$\begin{aligned} \chi_{yx}^{(i)}(\tau', v') &= \sqrt{L_i} e^{j2\pi v' \tau_i} \chi_{xx}^{(i)}(v', \tau') \\ &+ \sum_{\substack{s \neq i \\ s \geq 0}}^{S-1} \sqrt{L_s} e^{j2\pi(v' - \Delta v_s)\tau_s} \chi_{xx}^{(i)}(v - \Delta v_s, \tau' - \Delta\tau_s) \\ &+ \chi_{wx}^{(i)}(v', \tau') \end{aligned} \quad (7)$$

Therefore, we could find the contribution to the signal to noise ratio (SNR) of the signal of interest  $i$  from the other  $s$  satellites. As mentioned above, the peak of the displaced CAF correspond to  $v' = 0$  and  $\tau' = 0$ , therefore, we define the SINR setting  $v' = 0$  and  $\tau' = 0$  in the CAF:

$$\begin{aligned} \text{SINR}_i &= \frac{L_i P_{\text{TX}}}{\sum_{s \neq i}^{S-1} L_s |\chi_{xx}^{(i)}(\Delta v_s, \Delta\tau_s)|^2 + |\chi_{wx}^{(i)}(v_i, \tau_i)|^2} \\ &= \frac{1}{\sum_{s \neq i}^{S-1} \frac{L_s}{L_i} |\chi_{xx}^{(i)}(\Delta v_s, \Delta\tau_s)|^2 + \frac{\sigma^2}{P_{\text{TX}} L_i}} \end{aligned} \quad (8) \quad (9)$$

where we assumed the same transmission power across all satellites, denoted as  $P_{\text{TX}}$ , and the CAF of the receiver noise as  $|\chi_{wx}^{(i)}(v_i, \tau_i)|^2 = \sigma^2$ . This simplification incorporates the concept that the noise power is attenuated by the transmitted power normalised by the FSPL at the  $i$ -th satellite, represented as  $P_{\text{TX}} L_i$ . Consequently, the interference contribution of the remaining satellites to the  $i$ -th satellite SINR, depends on the distance ratio  $\rho$  as

$$I_i = \sum_{s \neq i}^{S-1} \left( \frac{\rho_s}{\rho_i} \right)^2 |\chi_{xx}^{(i)}(\Delta\tau_s, \Delta v_s)|^2. \quad (10)$$

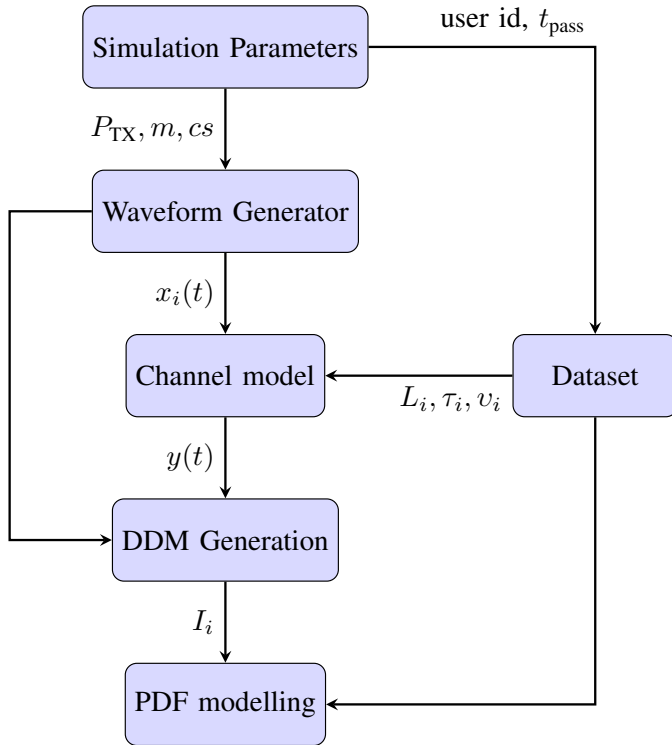


Figure 6: 5G PRS LEO simulator architecture.

This assumption is valid under the approximation that all satellites transmit at the same wavelength, which is the characteristic scenario using a common BWP for transmitting the PRS. Moreover, interference is further influenced by differential delay, denoted as  $\Delta\tau_s$ , and differential Doppler shift, represented as  $\Delta v_s$  between the satellite of interest  $i$  and the interfere satellite  $s$ . Deriving an analytical expression for  $I_i$  is rendered infeasible due to the nature of the integral involved and the characteristics of the distance dynamics. Consequently, to analyse the effects of interference in a comprehensive way, we have implemented a Monte Carlo simulation and extract a probability density function (PDF) for this interference.

#### IV. Interference modeling

This section describes the Monte Carlo simulator developed, the methodology to extract the interference model and the parameters models based on the PRS waveform configuration.

##### A. Monte Carlo simulator architecture

Figure 6 shows the simulator developed in order to extract the model for the PDF of the interference seen in equation (10). This simulator follows a Monte Carlo technique, evaluating the system for different user locations and signal configurations from the dataset [26]

The assumption taken for the simulator is that all the satellites are synchronized and transmit the PRS at the same

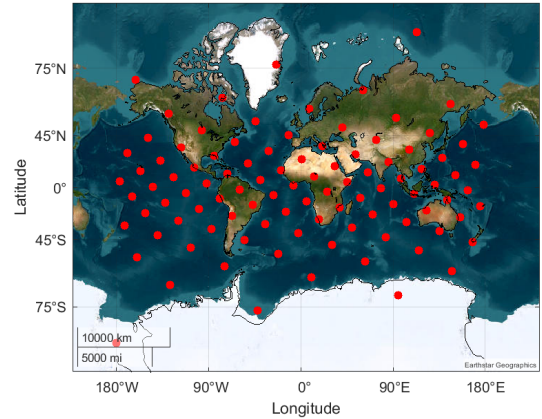


Figure 7: User's distribution of the dataset.

time but in a different RG arrangement, as seen previously in Figure 2. This simulator starts with the definition of the simulation parameters, such as the signal configuration and the dataset [26] for the satellite passes. Then it generates the waveforms requested. The next step is to apply to each waveform  $i$  the corresponding channel, where the delay  $\tau_i$ , losses  $L_i$  and Doppler  $v_i$  are tightly coupled due to satellite movement. They also are dependant on the user's latitude, as some latitudes have more probability to have more satellites in view than others such as the poles, mid-latitudes or the Equator. Then the simulator performs the signal acquisition, by computing the DDM of the received signal composed of the signal of interest and the other interference signals plus noise. Finally, from the DDM, the simulator generates the interference power samples used to analyze its probabilistic behavior.

The dataset used is available in [26], it has 100 users uniformly spread on Earth's surface (using a Fibonacci lattice). For each user location, 10 min of Starlink satellite passes are stored with 1 s resolution. Figure 7 shows the location of the users on Earth from the dataset used to compute the satellite passes.

The Monte Carlo simulator performs 1000 iterations per user location. For each iteration, the simulator took a random time to obtain the delay, Doppler, and distance between the user and 4 satellites that have an elevation angle greater than a selected mask  $\theta_{\text{MASK}} \leq \theta_i$ .

Table 1 enumerates the parameters relevant to the scenario delineated in Section II. In this scenario, the number of concurrent satellites in LOS is set to four, which represents the minimum required for a 3D position estimation. The bandwidth is designated as the minimum permissible for the transmission of the PRS. Similarly, the carrier frequency is chosen as the highest allowed within the n256 band.

Table 2 shows the different values of the parameters used to generate the PRS used in the simulation. We have made a comparison using different number of OFDM symbols,

Description	Symbol	Value
Number of satellite in LOS	$S$	4
Maximum signal bandwidth	$BW_{\text{MAX}}$	8.64 MHz
Satellite's constellation		Starlink. Inclination of 53 deg/554km
Transmitter power	$P_{\text{TX}}$	1,10,20,30 dBW
Carrier frequency	$f_c$	n256 (2.2 GHz)
Number of MC iterations	$N_{\text{index}}$	1000
Doppler Max value	$\pm v_{\text{MAX}}$	40 kHz
Doppler resolution	$v_{\text{step}}$	500 Hz

Table 1: Scenario details

Description	Symbol	Value
Number of Symbols	$m$	1 to 12
Number of Subcarriers	$N_{\text{SC}}$	288
Subcarrier Spacing	$\Delta f$	30 kHz
Comb Size	$cs$	4, 6 and 12

Table 2: PRS generation details.

different values of CombSize, and different transmission powers.

### B. Interference distribution model extraction

As seen in the previous Section III the statistical interference model in (10) used in the SINR analysis cannot be expressed in a closed form. Therefore, here we present the methodology for using the Monte Carlo approach to extract the distribution of the interference created by the PRS. Figure 8 illustrates a comparison between two examples empirical cumulative density function (ECDF) for two waveform configurations. One is using one symbol OFDM and the other uses 12 symbols, both with a comb size of 4 and a transmission power of 30 dBW. The plot reveals that with an 80% probability, using one symbol, the interference power will be at least  $-170$  dBW, while using 12 symbols, these values increase up to  $-150$  dBW.

To find the probability distribution that best describes this behavior, a Kolmogorov-Smirnov test (KS) metric is used to evaluate the fitness of the measurement samples to a tested distribution. The ECDF obtained from the interference power samples in the simulator are compared to different distributions, and among them the one with the lowest KS metric is selected to model it. This KS metric is the largest distance between the ECDF of the samples and the cumulative density function (CDF) of the different distributions tested.

$$D_{n,m} = \sup_x |F_n(x) - G_m(x)| \quad (11)$$

Where  $F_n(x)$  and  $G_m(x)$  are the ECDF of the samples and the CDF of the distribution under test. To this test, we have added the p-value of the KS test as it indicates the probability of obtaining test results at least as extreme as the observed

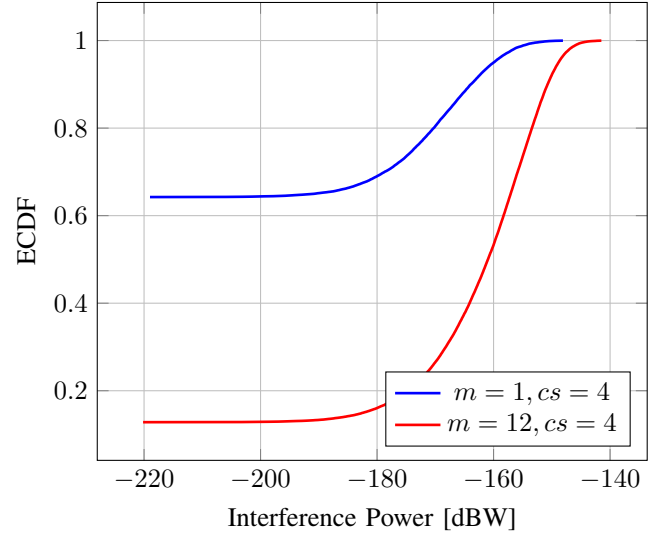


Figure 8: ECDF comparison between using 1 or 12 symbol OFDM and a CombSize of 4.

Distribution	KS	p-test
Normal	0.0382	0
LogNormal	0.0256	0
Gamma	0.0298	0
Rayleigh	0.5295	0
Rician	0.0382	0
Generalized extreme value (GEV)	0.0142	0.368

Table 3: KS test result for the different distribution tested.

results, under the assumption that the null hypothesis (the sample follows the reference distribution) is true. A higher p-value indicates a better fit to the distribution. Table 3 shows the KS fitness test and p-value for the different distribution used to test. The distribution that best fits the measurements corresponds to the lower KS statistic of 0.0142 and the highest p-value of 0.3688 corresponds to a GEV distribution. The CDF expression for this GEV distribution is described as

$$F_{\text{Interference}}(x) = \exp \left( - \left[ 1 + k \left( \frac{x - \mu}{\sigma} \right) \right]^{-1/k} \right). \quad (12)$$

This GEV distribution is defined by 3 parameters:  $k$  or shape,  $\sigma$  or scale, and  $\mu$  or location. Figure 9 shows in blue the empirical PDF for two different waveform configurations (using 1 and 12 OFDM symbols) and with different colors, in red, the fitted PDF using a GEV model. Once the distribution that best fits the samples is found, we derive an empirical model to link the PRS configuration settings with the distribution parameters. Each parameter of the GEV,  $[k, \mu, \sigma]$ , depends on the PRS configuration such as the number of symbols  $m$ , comb size  $cs$ , and transmitted power  $P_{\text{TX}}$ . Figure 10 shows that the value of  $\mu$  depends on the number of symbols  $m$  and the transmitted power  $P_{\text{TX}}$ . It is modeled by

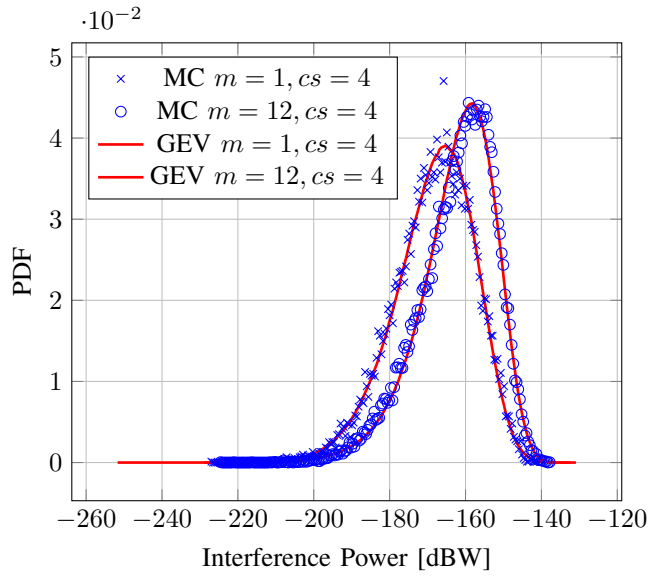


Figure 9: Example of a PDF of the Interference power to compare the results from the Monte Carlo and the GEV distribution.

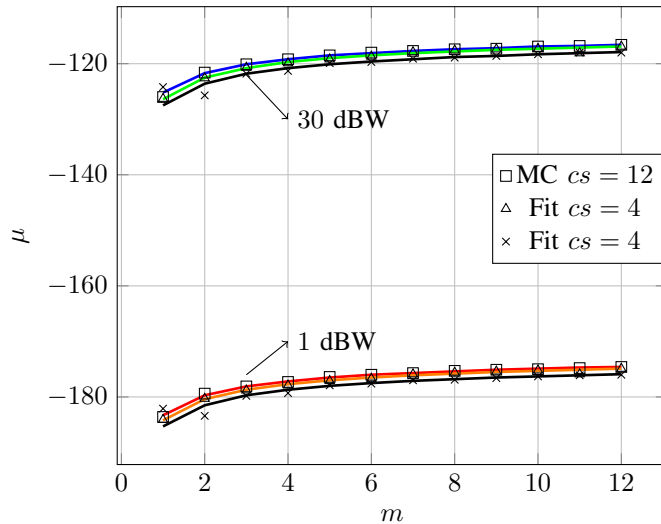


Figure 10: GEV  $\mu$  fitting for different OFDM symbols, comb size and  $P_{TX}$  parameters.

$\mu(m, P_{TX}) = \frac{a_1}{\sqrt{m}} + a_2 P_{TX} + a_3$ . Then, to extract the values for  $a_1, a_2, a_3$  we apply a change of variable  $u = \frac{1}{\sqrt{m}}$ . The equation can be written in matrix form as  $\mathbf{F} = \mathbf{X}\beta$  where:

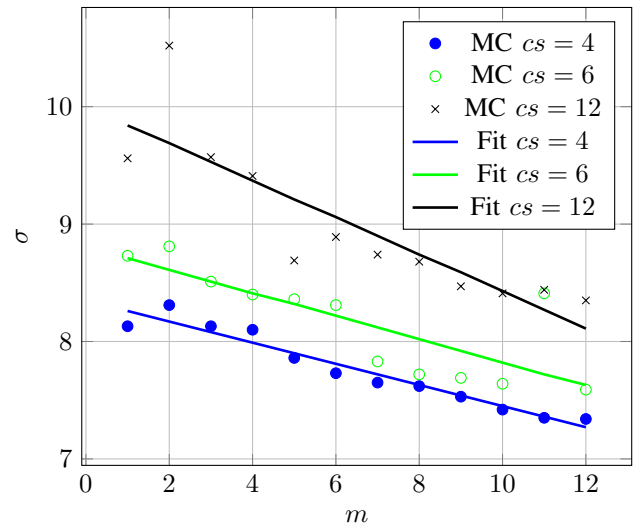


Figure 11: GEV  $\sigma$  fitting for different OFDM symbols and comb size parameters.

cs	$a_1$	$a_2$	$a_3$	$b_1$	$b_2$	$c_1$	$c_2$
4	0.629	1.99	-182	-0.090	8.35	-0.185	0.038
6	0.643	1.99	-183	-0.098	8.80	-0.229	0.044
12	0.612	2.00	-184	-0.157	10	-0.172	-0.011

Table 4: Values of the parameters to generate  $[k(m), \mu(m, P_{TX}), \sigma(m)]$  of the GEV for the interference of the PRS.

$$\mathbf{F} = \begin{pmatrix} \mu_1 \\ \mu_2 \\ \vdots \\ \mu_z \end{pmatrix}, \quad \mathbf{X} = \begin{pmatrix} 1 & P_{TX1} & 1 \\ \frac{1}{\sqrt{2}} & P_{TX1} & 1 \\ \vdots & \vdots & \vdots \\ \frac{1}{\sqrt{12}} & P_{TX1} & 1 \\ 1 & P_{TX2} & 1 \\ \frac{1}{\sqrt{2}} & P_{TX2} & 1 \\ \vdots & \vdots & \vdots \\ \frac{1}{\sqrt{12}} & P_{TX2} & 1 \\ \vdots & \vdots & \vdots \\ 1 & P_{TXn} & 1 \\ \frac{1}{\sqrt{2}} & P_{TXn} & 1 \\ \vdots & \vdots & \vdots \\ \frac{1}{\sqrt{12}} & P_{TXn} & 1 \end{pmatrix}, \quad \beta = \begin{pmatrix} a_1 \\ a_2 \\ a_3 \end{pmatrix} \quad (13)$$

and we solve for  $\beta$  using least squares (LS) as  $\beta = (\mathbf{X}^T \mathbf{X})^{-1} \mathbf{X}^T \mu$ . Then we model  $\sigma$  from the results as a linear model  $\sigma(m) = b_1 m + b_2$  as seen in Figure 11. The last parameter we model is  $k$ , from the results they follow a curve  $k(m) = \frac{c_1}{\sqrt{m}} + c_2$ , as seen in Figure 12. Finally, table 4 presents the values for the different parameters to generate  $[k(m), \mu(m, P_{TX}), \sigma(m)]$  for the GEV. This model extraction can be used in future simulations to evaluate the

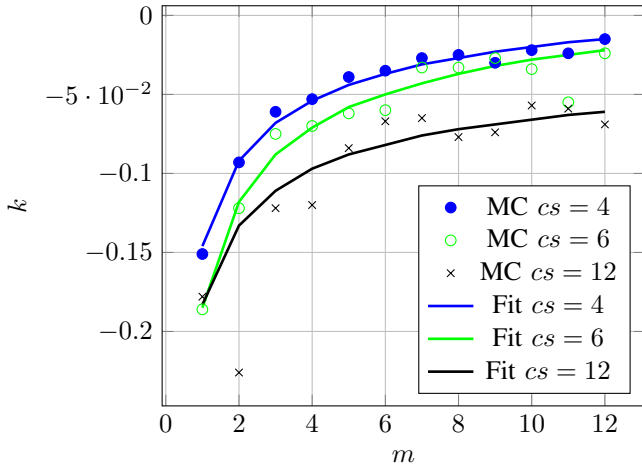


Figure 12: GEV  $k$  fitting for different OFDM symbols and comb size parameters.

interference power that a PRS pilot will generate in a typical scenario with reception from 4 satellites.

## V. Conclusions and Prospects for Future Research

This study presents a model of the interference power in a NTN scenario when using the PRS as a signal for positioning. The model has been extracted empirically using a Monte Carlo approach as the dynamics of the LEO scenario makes it unfeasible to have a direct mathematical formulation for interference modeling. Two analytical tools, the CAF and the DDM, have been used in assessing the interference for a PRS signal. These methodologies have paved the way for an open research question: the feasibility of designing a positioning system that multiplexes different transmissions while minimizing interference. In summary, the findings of this study contribute significantly to the understanding of interference challenges in LEO scenarios. They mark a step towards the integration of 5G NTN as an autonomous system, independent of GNSS receivers at the UE end. The results highlight the need for advanced multiplexing strategies to manage multiple satellite signals within the same BWP, thereby mitigating SINR degradation. Future research includes applying a precompensation to delay and Doppler within the beam coverage area, including the ICI and ISI model during the DDM computation to reduce their effects, or exploring alternative waveform designs such as orthogonal time frequency space modulation (OTFS), which could leverage their robustness in high Doppler and delay environments. Another avenue for enhancing current results involves the implementation of a successive interference cancellation (SIC) algorithm, which holds promise for improving the SINR of the signal [30], or exploit the sparsity of the DDM matrix by using an orthogonal matching pursuit (OMP) algorithm.

## Appendix. Acronyms

This paper makes use of an extensive number of acronyms, and to help the reader, the following list shows all of them:

<b>5G</b>	fifth generation
<b>3GPP</b>	3rd Generation Partnership Project
<b>AF</b>	ambiguity function
<b>BWP</b>	bandwidth part
<b>BWPP</b>	bandwidth part for positioning
<b>CAF</b>	cross ambiguity function
<b>CDF</b>	cumulative density function
<b>CP</b>	cyclic prefix
<b>CP-OFDM</b>	cyclic prefix orthogonal frequency-division modulation
<b>DDM</b>	delay/Doppler map
<b>ECDF</b>	empirical cumulative density function
<b>EIRP</b>	equivalent isotropic radiated power
<b>FFR</b>	fraction frequency reuse
<b>FoV</b>	field of view
<b>FR1</b>	frequency region 1
<b>FR2</b>	frequency region 2
<b>FSPL</b>	free space path loss
<b>GEV</b>	Generalized extreme value
<b>gNB</b>	next generation base station
<b>GNSS</b>	global navigation satellite system
<b>HAPS</b>	high-altitude platform systems
<b>HPA</b>	high power amplifier
<b>IFFT</b>	inverse fast Fourier transform
<b>IoT</b>	Internet of things
<b>ICI</b>	inter-carrier interference
<b>INI</b>	inter-numerology interference
<b>ISI</b>	inter-symbol interference
<b>KPI</b>	key performance indicator
<b>KS</b>	Kolmogorov-Smirnov test
<b>LEO</b>	low Earth orbit
<b>LOS</b>	line of sight
<b>LS</b>	least squares
<b>LTE</b>	Long Term Evolution
<b>NTN</b>	non-terrestrial network
<b>OFDM</b>	orthogonal frequency-division multiplexing
<b>OMP</b>	orthogonal matching pursuit
<b>OTFS</b>	orthogonal time frequency space modulation
<b>PDF</b>	probability density function
<b>PNT</b>	positioning, navigation, and timing
<b>PRS</b>	positioning reference signal
<b>RE</b>	resource element
<b>RG</b>	resource grid
<b>SIC</b>	successive interference cancellation
<b>SINR</b>	signal to interference plus noise ratio
<b>SNO</b>	satellite network operator
<b>SNR</b>	signal to noise ratio
<b>SSP</b>	subsatellite point
<b>ToA</b>	time of arrival
<b>UAV</b>	unmanned aerial vehicle
<b>UE</b>	user equipment
<b>WSS</b>	wide-sense stationary

## Acknowledgement

**Acknowledgments:** The simulations presented in this paper were carried out using the HPC facilities of the University of Luxembourg [31] (see [hpc.uni.lu](http://hpc.uni.lu)).

The work presented in this paper was carried out in the framework of SatNEx V WI 3.3: LEO-PNT project, funded by ESA. contract no. 4000130962/20/NL/NL/FE. The authors thank Dr. Nader Alagha from ESA for his constructive discussions. The views expressed in this paper can in no way be taken to reflect the official opinion of the European Space Agency.

## References

- [1] M. El Jaafari, N. Chuberre, S. Anjuere, and L. Combelles, "Introduction to the 3GPP-defined NTN standard: A comprehensive view on the 3GPP work on NTN," *International Journal of Satellite Communications and Networking*, vol. 41, no. 3, pp. 220–238, 2023, eprint: <https://onlinelibrary.wiley.com/doi/pdf/10.1002/sat.1471>. [Online]. Available: <https://onlinelibrary.wiley.com/doi/abs/10.1002/sat.1471>
- [2] "Study on NR positioning support," 3GPP, Technical Report (TR) 38.855, 2019. [Online]. Available: <https://portal.3gpp.org/desktopmodules/Specifications/SpecificationDetails.aspx?specificationId=3501>
- [3] I. Muursepp, M. Kulmar, O. Elghary, M. M. Alam, T. Chen, S. Horsmanheimo, and J. Scholliers, "Performance Evaluation of 5G-NR Positioning Accuracy Using Time Difference of Arrival Method," in *2021 IEEE International Mediterranean Conference on Communications and Networking (MeditCom)*. Athens, Greece: IEEE, Sep. 2021, pp. 494–499. [Online]. Available: <https://ieeexplore.ieee.org/document/9647652/>
- [4] M. Panchetti, C. Carbonelli, M. Horvat, and M. Luise, "Performance analysis of PRS-based synchronization algorithms for LTE positioning applications," in *2013 10th Workshop on Positioning, Navigation and Communication (WPNC)*. Dresden: IEEE, Mar. 2013, pp. 1–6. [Online]. Available: <http://ieeexplore.ieee.org/document/6533292/>
- [5] F. Rinaldi, H.-L. Maattanen, J. Torsner, S. Pizzi, S. Andreev, A. Iera, Y. Koucheryavy, and G. Araniti, "Non-Terrestrial Networks in 5G & Beyond: A Survey," *IEEE Access*, vol. 8, pp. 165 178–165 200, 2020, conference Name: IEEE Access.
- [6] S. E. Trevlakis, A.-A. A. Boulogeorgos, D. Pliatsios, J. Querol, K. Ntontin, P. Sarigiannidis, S. Chatzinotas, and M. Di Renzo, "Localization as a Key Enabler of 6G Wireless Systems: A Comprehensive Survey and an Outlook," *IEEE Open Journal of the Communications Society*, vol. 4, pp. 2733–2801, 2023, conference Name: IEEE Open Journal of the Communications Society. [Online]. Available: <https://ieeexplore.ieee.org/document/10287134/references#references>
- [7] H. K. Dureppagari, C. Saha, H. S. Dhillon, and R. M. Buehrer, "NTN-based 6G Localization: Vision, Role of LEOs, and Open Problems," Sep. 2023, arXiv:2305.12259 [cs, eess, math]. [Online]. Available: <http://arxiv.org/abs/2305.12259>
- [8] Z. Wei, Y. Wang, L. Ma, S. Yang, Z. Feng, C. Pan, Q. Zhang, Y. Wang, H. Wu, and P. Zhang, "5G PRS-Based Sensing: A Sensing Reference Signal Approach for Joint Sensing and Communication System," *IEEE Transactions on Vehicular Technology*, vol. 72, no. 3, pp. 3250–3263, Mar. 2023, conference Name: IEEE Transactions on Vehicular Technology.
- [9] W. A. Martins, F. Cruz-Roldán, M. Moonen, and P. S. Ramirez Diniz, "Intersymbol and Intercarrier Interference in OFDM Transmissions Through Highly Dispersive Channels," in *2019 27th European Signal Processing Conference (EUSIPCO)*, Sep. 2019, pp. 1–5, iSSN: 2076-1465.
- [10] F. Cruz-Roldán, W. A. Martins, F. G. G., M. Moonen, and P. S. R. Diniz, "Intersymbol and Intercarrier Interference in OFDM Systems: Unified Formulation and Analysis," Dec. 2020, arXiv:2012.04527 [eess]. [Online]. Available: <http://arxiv.org/abs/2012.04527>
- [11] M. Nematı and H. Arslan, "Low ICI Symbol Boundary Alignment for 5G Numerology Design," *IEEE Access*, vol. 6, pp. 2356–2366, 2018, conference Name: IEEE Access.
- [12] L. Marijanović, S. Schwarz, and M. Rupp, "Multiplexing Services in 5G and Beyond: Optimal Resource Allocation Based on Mixed Numerology and Mini-Slots," *IEEE Access*, vol. 8, pp. 209 537–209 555, 2020, conference Name: IEEE Access.
- [13] A. B. Kihero, M. S. J. Solaija, and H. Arslan, "Inter-Numerology Interference for Beyond 5G," *IEEE Access*, vol. 7, pp. 146 512–146 523, 2019. [Online]. Available: <https://ieeexplore.ieee.org/document/8861343/>
- [14] S. A. Khan, A. Kavak, s. Aldirmaz Çolak, and K. Küçük, "A Novel Fractional Frequency Reuse Scheme for Interference Management in LTE-A HetNets," *IEEE Access*, vol. 7, pp. 109 662–109 672, 2019, conference Name: IEEE Access. [Online]. Available: <https://ieeexplore.ieee.org/document/8790698>
- [15] S. Venkatesan, A. Lozano, and R. Valenzuela, "Network MIMO: Overcoming Intercell Interference in Indoor Wireless Systems," in *2007 Conference Record of the Forty-First Asilomar Conference on Signals, Systems and Computers*, Nov. 2007, pp. 83–87, iSSN: 1058-6393. [Online]. Available: <https://ieeexplore.ieee.org/document/4487170>
- [16] N. Trabelsi, L. C. Fourati, and C. S. Chen, "Interference Management in 5G and Beyond Networks," Jan. 2024, arXiv:2401.01608 [cs, eess, math]. [Online]. Available: <http://arxiv.org/abs/2401.01608>
- [17] L. Zhen, A. K. Bashir, K. Yu, Y. D. Al-Otaibi, C. H. Foh, and P. Xiao, "Energy-Efficient Random Access for LEO Satellite-Assisted 6G Internet of Remote Things," *IEEE Internet of Things Journal*, vol. 8, no. 7, pp. 5114–5128, Apr. 2021, conference Name: IEEE Internet of Things Journal. [Online]. Available: <https://ieeexplore.ieee.org/document/9222142>
- [18] X. Lin, J. Bergman, F. Gunnarsson, O. Liberg, S. M. Razavi, H. S. Razaghi, H. Rydn, and Y. Sui, "Positioning for the Internet of Things: A 3GPP Perspective," *IEEE Communications Magazine*, vol. 55, no. 12, pp. 179–185, Dec. 2017, conference Name: IEEE Communications Magazine. [Online]. Available: <https://ieeexplore.ieee.org/document/8030544>
- [19] W. Sixin, T. Xiaomei, L. Xiaohui, F. Wang, and Z. Zhuang, "Doppler frequency-code phase division multiple access technique for LEO navigation signals," *GPS Solutions*, vol. 26, no. 3, p. 98, Jun. 2022. [Online]. Available: <https://doi.org/10.1007/s10291-022-01283-7>
- [20] S. Dwivedi, R. Shreevastav, F. Munier, J. Nygren, I. Siomina, Y. Lyazidi, D. Shrestha, G. Lindmark, P. Ernstrom, E. Stare, S. M. Razavi, S. Muruganathan, G. Masini, A. Busin, and F. Gunnarsson, "Positioning in 5G Networks," *IEEE Communications Magazine*, vol. 59, no. 11, pp. 38–44, Nov. 2021, conference Name: IEEE Communications Magazine. [Online]. Available: <https://ieeexplore.ieee.org/document/9665436>
- [21] P. J. Honnaiah, E. Lagunas, S. Chatzinotas, and J. Krause, "Demand-Driven Beam Densification in Multibeam Satellite Communication Systems," *IEEE Transactions on Aerospace and Electronic Systems*, vol. 59, no. 5, pp. 6534–6554, Oct. 2023, conference Name: IEEE Transactions on Aerospace and Electronic Systems. [Online]. Available: <https://ieeexplore.ieee.org/document/10130323>
- [22] Y. Hong, T. Thaj, and E. Viterbo, *Delay-Doppler communications principles and applications*. London: Academic Press, an imprint of Elsevier, 2022, oCLC: 1297827135.
- [23] J. A. Klobuchar, "Ionospheric Time-Delay Algorithm for Single-Frequency GPS Users," *IEEE Transactions on Aerospace and Electronic Systems*, vol. AES-23, no. 3, pp. 325–331, May 1987, conference Name: IEEE Transactions on Aerospace and Electronic Systems. [Online]. Available: <https://ieeexplore.ieee.org/document/4104345>
- [24] G. Di Giovanni and S. M. Radicella, "An analytical model of the electron density profile in the ionosphere," *Advances in Space Research*, vol. 10, no. 11, pp. 27–30, Jan. 1990. [Online]. Available: <https://www.sciencedirect.com/science/article/pii/027311779090301F>
- [25] J. Sanz Subirana, J. M. Juan Zornoza, and M. Hernández-Pajares, *GNSS DATA Processing, Fundamentals and algorithms. Vol. 1*. Noordwijk: ESA Communications, 2013, oCLC: 922681096.
- [26] A. Gonzalez-Garrido, "Starlink satellite passes," 2024, text entry type: data. [Online]. Available: <https://dx.doi.org/10.21227/qggt-xr49>
- [27] V. M. Baeza, E. Lagunas, H. Al-Hraishawi, and S. Chatzinotas, "An Overview of Channel Models for NGSO Satellites," in *2022 IEEE 96th Vehicular Technology Conference (VTC2022-Fall)*, Sep. 2022, pp. 1–6, iSSN: 2577-2465. [Online]. Available: <https://ieeexplore.ieee.org/document/10012693>

- [28] 3GPP, “NR; Physical channels and modulation,” 3GPP, Technical Specification (TS) 38.211, 2024. [Online]. Available: <https://portal.3gpp.org/desktopmodules/Specifications/SpecificationDetails.aspx?specificationId=3213>
- [29] J. Querol, A. Alonso-Arroyo, R. Onrubia, D. Pascual, H. Park, and A. Camps, “SNR Degradation in GNSS-R Measurements Under the Effects of Radio-Frequency Interference,” *IEEE Journal of Selected Topics in Applied Earth Observations and Remote Sensing*, vol. 9, no. 10, pp. 4865–4878, Oct. 2016, conference Name: IEEE Journal of Selected Topics in Applied Earth Observations and Remote Sensing.
- [30] N. I. Miridakis and D. D. Vergados, “A Survey on the Successive Interference Cancellation Performance for Single-Antenna and Multiple-Antenna OFDM Systems,” *IEEE Communications Surveys & Tutorials*, vol. 15, no. 1, pp. 312–335, 2013, conference Name: IEEE Communications Surveys & Tutorials.
- [31] S. Varrette, H. Cartiaux, S. Peter, E. Kieffer, T. Valette, and A. Olloh, “Management of an academic HPC & research computing facility: The ULHPC experience 2.0,” in *Proc. of the 6th ACM high performance computing and cluster technologies conf. (HPCCT 2022)*. Fuzhou, China: Association for Computing Machinery (ACM), Jul. 2022.

and Technology Hellas and Mobile Communications Research Group, Center of Communication Systems Research, University of Surrey. He has received the M.Eng. in Telecommunications from Aristotle University of Thessaloniki, Greece and the M.Sc. and Ph.D. in Electronic Engineering from University of Surrey, UK in 2003, 2006 and 2009 respectively. He has authored more than 700 technical papers in refereed international journals, conferences and scientific books and has received numerous awards and recognitions, including the IEEE Fellowship and an IEEE Distinguished Contributions Award. He is currently in the editorial board of the IEEE Transactions on Communications, IEEE Open Journal of Vehicular Technology and the International Journal of Satellite Communications and Networking.



**Alejandro Gonzalez-Garrido** PhD Student at SIGCOM group from SnT, (University of Luxembourg) in hybrid GNSS and 5G PNT systems using Non-Terrestrial Networks. Integrated degree plus M.Sc. in Telecommunication Engineering obtained in 2015. With professional experience in the timing and synchronization industry, satellite design, and network operations.



**Jorge Querol** received his Ph.D degree in telecommunication engineering, from the Polytechnic University of Catalonia (UPC-BarcelonaTech), Barcelona (Spain), in 2018. His research interests include Software Defined Radios (SDR), real-time signal processing, satellite communications, satellite navigation and remote sensing. Jorge joined the Signal Processing and Satellite Communications group, SIGCOM, headed by Prof. Björn Ottersten and he will be working with Dr. Symeon Chatzinotas.



gence of communication

**Henk Wymeersch** (S’01, M’05, SM’19, F’24) obtained the Ph.D. degree in Electrical Engineering/Applied Sciences in 2005 from Ghent University, Belgium. He is currently a Professor of Communication Systems with the Department of Electrical Engineering at Chalmers University of Technology, Sweden. He is Senior Member of the IEEE Signal Processing Magazine Editorial Board. During 2019-2021, he was an IEEE Distinguished Lecturer with the Vehicular Technology Society. His current research interests include the convergence of communication and sensing, in a 5G and Beyond 5G context.



**Symeon Chatzinotas** (MEng, MSc, PhD, FIEEE) is currently Full Professor / Chief Scientist I and Head of the research group SIGCOM in the Interdisciplinary Centre for Security, Reliability and Trust, University of Luxembourg.

In the past, he has lectured as Visiting Professor at the University of Parma, Italy and contributed in numerous R&D projects for the Institute of Informatics & Telecommunications, National Center for Scientific Research “Demokritos” the Institute of Telematics and Informatics, Center of Research